ADVANCED FUNCTIONAL MATERIALS
www.afm-journal.de



# High-Mobility ZnO Thin Film Transistors Based on Solution-processed Hafnium Oxide Gate Dielectrics

*Mazran Esro, George Vourlias, Christopher Somerton, William I. Milne, and George Adamopoulos**

**The properties of metal oxides with high dielectric constant (*k*) are being extensively studied for use as gate dielectric alternatives to silicon dioxide ($SiO_2$). Despite their attractive properties, these high-*k* dielectrics are usually manufactured using costly vacuum-based techniques. In that respect, recent research has been focused on the development of alternative deposition methods based on solution-processable metal oxides. Here, the application of the spray pyrolysis (SP) technique for processing high-quality hafnium oxide ($HfO_2$) gate dielectrics and their implementation in thin film transistors employing spray-coated zinc oxide (ZnO) semiconducting channels are reported. The films are studied by means of admittance spectroscopy, atomic force microscopy, X-ray diffraction, UV–Visible absorption spectroscopy, FTIR, spectroscopic ellipsometry, and field-effect measurements. Analyses reveal polycrystalline $HfO_2$ layers of monoclinic structure that exhibit wide band gap (≈5.7 eV), low roughness (≈0.8 nm), high dielectric constant ($k \approx 18.8$), and high breakdown voltage (≈2.7 MV/cm). Thin film transistors based on $HfO_2$/ZnO stacks exhibit excellent electron transport characteristics with low operating voltages (≈6 V), high on/off current modulation ratio (~$10^7$) and electron mobility in excess of 40 $cm^2 V^{-1} s^{-1}$.**

## 1. Introduction

The high optical transparency and excellent charge transport characteristics combined with their excellent chemical stability and mechanical tolerance make metal oxides semiconductors attractive for applications in large area optoelectronics and particularly thin film transistors (TFTs). Despite their short history, metal oxide semiconductor based thin-film transistors[1–3] have already been demonstrated with high performance comparable to polycrystalline silicon.[4,5] Nevertheless, those high-performance metal oxide-based TFTs are usually manufactured using costly vacuum-based techniques.[6,7] To address this problem, recent research has been focused on the development of TFTs using alternative deposition methods based on solution-processed oxide semiconductors.[8–14]

Along with the progress on solution-processed metal oxide semiconductors, research towards solution processed gate dielectrics based on high-*k* or electrolyte dielectrics has also been boosted.[12,15–19] However the vast majority of the reported work employs conventional dielectrics based on $SiO_2$. Amongst high-*k* dielectrics that include a wide range of transition metals[20,21] and rare earth[22,23] metal oxides, hafnium oxide ($HfO_2$) is one of the most extensively studied material as a gate dielectric due to its high dielectric constant and wide band gap. $HfO_2$ thin films can be grown using a wide range of vacuum based deposition techniques namely the atomic layer deposition (ALD),[24,25] chemical vapor deposition (CVD),[26,27] magnetron sputtering,[28–30] pulsed laser deposition (PLD)[29–32] and molecular beam epitaxy (MBE).[33] $HfO_2$ films deposition from solutions have also been reported.[34–37] However the preferred industrial scale methods are CVD and ALD.

In this report we demonstrate the deposition of $HfO_2$ gate dielectrics using a simple and large area compatible technique namely spray pyrolysis (SP). $HfO_2$ dielectrics were deposited onto antimony-doped tin oxide coated glass, fused silica, KBr, and c-Si substrates. The film properties were investigated using a wide range of characterization techniques including UV–Vis absorption spectroscopy, spectroscopic ellipsometry, admittance spectroscopy, X-ray diffraction, AFM, and FTIR. TFT characteristics were obtained from optimized bottom-gate, top-contact transistor architecture employing spray coated $HfO_2$ gate dielectric and ZnO semiconducting channels.

M. Esro, Dr. G. Adamopoulos
Engineering Department
Lancaster University
Lancaster LA1 4YR, UK
E-mail: g.adamopoulos@lancaster.ac.uk
Dr. G. Vourlias
Physics Department
Aristotle University of Thessaloniki
Thessaloniki 54142, Greece
Dr. C. Somerton
Quantum Technology Centre
Department of Physics
University of Lancaster
LA1 4YW, UK
Prof. W. I. Milne
Department of Engineering
University of Cambridge
9 JJ Thomson Avenue, Cambridge CB3 0FA, UK
Prof. W. I. Milne
Kyung Hee University
Display Research Laboratory
Department of Information Display
Seoul 130701, South Korea

DOI: 10.1002/adfm.201402684

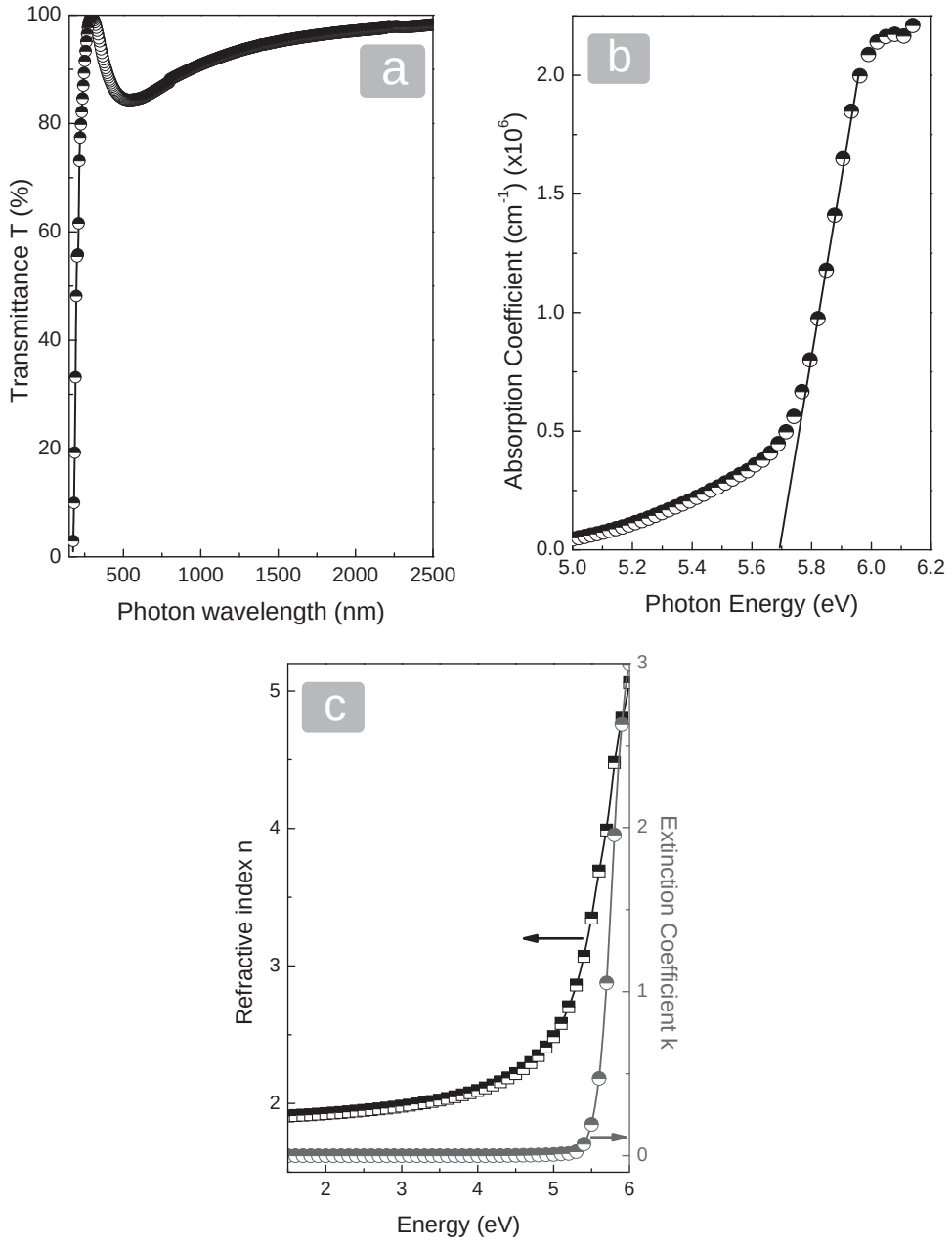


**Figure 1.** a) Transmittance T% of $HfO_2$ sprayed at 450 °C on fused silica substrates. b) The Tauc plot of the $HfO_2$ film. c) Refractive index and extinction coefficient of $HfO_2$ films spray coated at 450 °C on Si as derived from spectroscopic ellipsometry.

## 2. Results and Discussion

### 2.1. Optical Properties of $HfO_2$ Films

The UV–Vis transmission spectra of $HfO_2$ films grown on fused silica substrates are shown in **Figure 1**a. The spectra clearly demonstrate films of high optical transmittance. The onset of the optical transitions of the $HfO_2$ films near the band edge is illustrated in Figure 1b by the Tauc plot[38] that shows a direct optical band gap of ≈5.7 eV.

The optical properties of $HfO_2$ films were investigated independently by ex situ UV–visible spectroscopic ellipsometry within the range of photon energies from 1.5 to 6 eV. Parameterization of optical constants in the UV–visible range is based on the fact that the energy dependent dielectric function $\varepsilon(E)$ of a semiconductor can be expressed by the contributions of band-to-band optical transitions that can be taken into account by Lorentzian oscillators. For $HfO_2$ films, one Lorentz oscillator was found to yield a good fit to the data. The use of one Lorentz oscillator is also consistent with material's electronic structure

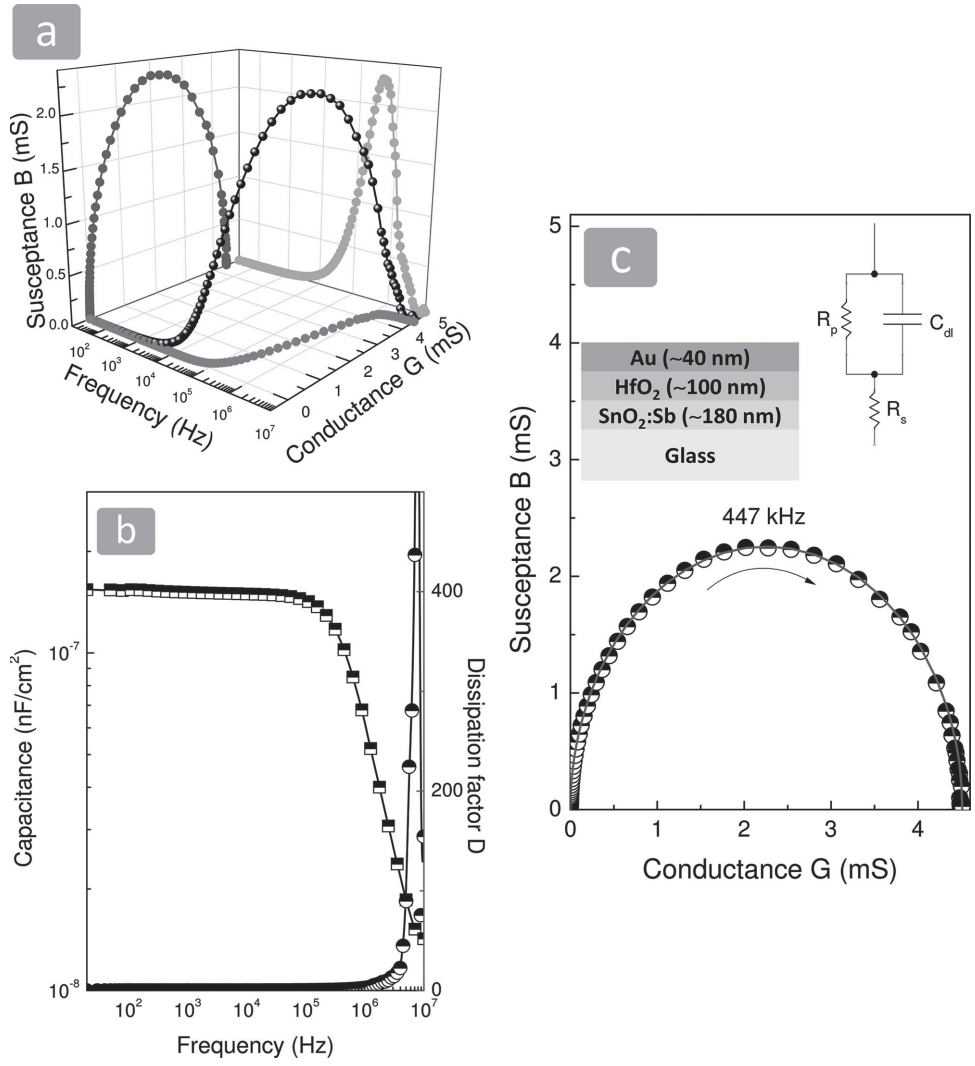


**Figure 2.** a) Susceptance and conductance dispersions of $HfO_2$ MIM structures at the frequency range between 20 Hz and 10 MHz. b) Capacitance and dissipation factor of spray coated ≈104 nm thick $HfO_2$ dielectric. c) Nyquist plot and equivalent circuit (inset) of $HfO_2$ MIM device.

and takes into account contributions from high energy band-to-band transitions. The refractive index ($n$) and extinction coefficient ($k$) dispersions are illustrated in Figure 1c. The derived optical band gap was found to be of ≈5.7 eV consistent with the value obtained from UV–Vis absorption spectroscopy. Additionally, the static dielectric constant ($k$) as well as the infinite dielectric constant ($\varepsilon_\infty$) were found to be ≈18.5 and ≈3.9 respectively. The latter value indicates a capacitance of ≈155 nF/cm$^2$ and pinning factor S of ≈0.54.[39–41]

### 2.2. $HfO_2$ Dielectric Properties and Leakage Currents

The current–voltage characteristics and dielectric properties of $HfO_2$ films were assessed by employing a metal-insulator-metal (MIM) device architecture. $HfO_2$ films of thickness of ≈104 nm were sandwiched between $SnO_2$:Sb and Au electrodes ($SnO_2$:Sb(180 nm)/$HfO_2$(104 nm)/Au(50 nm)). The susceptance ($B$) and conductance ($G$) spectra in the frequency range between 20 Hz and 10 MHz are shown in **Figure 2**a. The recorded capacitance $C_{ox}$, dissipation factor (D), as well as the Nyquist plots and equivalent circuit are illustrated in Figure 2b and Figure 2c respectively.

The static dielectric constant $k$ of ≈18.8 as extracted from admittance spectroscopy was also found to be in good agreement with the one that was extrapolated from spectroscopic ellipsometry. Also, the geometric capacitance at 100 Hz extracted from the Bode plot was found to be 151 nF/cm$^2$ in very good agreement with the theoretical one derived from the spectroscopic ellipsometry (assuming $k \approx 18.5$). The dissipation factor that was found to be less than 0.01 at low frequencies shows a resonance at about 8 MHz that may be attributed to dipole relaxation at high frequencies. In addition, the equivalent circuit (inset Figure 2c) derived from admittance spectroscopy data analysis show excellent capacitive properties in terms of high shunt (≈1 GOhm) and low series resistance

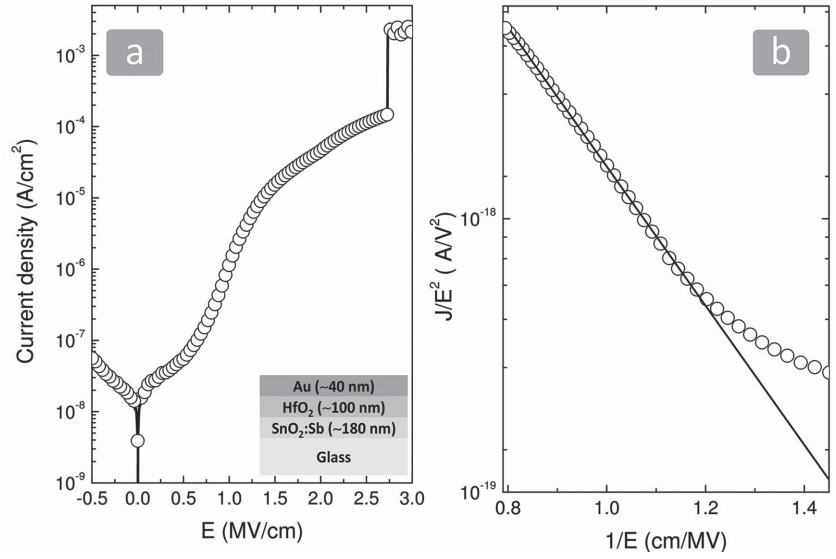


**Figure 3.** a) Leakage current density and b) F-N plot of a ≈104 nm $HfO_2$ MIM device deposited by SP.

(≈25 Ohms). The current-density and electric field characteristics of the same stacks ($SnO_2$:Sb(180 nm)/$HfO_2$(105 nm)/Au(50 nm)) are shown in **Figure 3**a. As shown, the devices exhibit very low leakage currents (<74 nA cm$^{-2}$ @ 6 V) with a dielectric breakdown around 2.7 MV cm$^{-1}$.

Figure 3b shows the Fowler Nordheim (F-N) plots of the same device. The linearity of the F-N plot over a wide $J/E^2$ range demonstrates that the conduction is indeed determined by F-N tunneling indicating an interface limited process.[42,43]

As mentioned before, one of the gate requirements is that the oxide's $k$ value should be high enough, preferably in the range between 25 and 30. There is however a trade off with the band offset condition (potential barrier at each band must be over 1 eV in order to inhibit conduction by the Schottky emission of electrons or holes into the oxide bands),[39] which requires a reasonably large band gap. It is known that the static dielectric constant of candidate oxides tends to vary inversely with the band gap[40,44] so for wide band gap semiconducting channels, such as ZnO, a relatively low $k$ value should be accepted. To note however that even in the case of narrow band gap semiconducting channels, a very large $k$ is unfavorable as it may cause undesirable large fringing fields at the source and drain electrodes.

**Figure 4** summarizes the band gap and static dielectric constant of a wide range of candidate materials as gate dielectrics grown by a wide range of deposition techniques.[42,45–50] Figure 4 clearly demonstrates universal dielectric constant-band gap correlation of both vacuum and solution processed gate dielectrics.

### 2.3. Structural Characterization of $HfO_2$ and $SnO_2$:Sb/$HfO_2$/ZnO Stacks

The microstructure of the spray coated $SnO_2$:Sb gate electrodes, $HfO_2$ gate dielectric, ZnO semiconducting channel and $SnO_2$:Sb/$HfO_2$/ZnO stack were investigated by X-ray diffraction. The raw grazing incidence (GIXRD) diffraction patterns are illustrated in **Figure 5**. Prior to data analysis, the background, mainly due to the glass substrate contribution, was subtracted using the Sonnerveld method.[51] Peak positions were determined by fitting the diffraction pattern data to a pseudo-Voight function. Basal spacings were obtained using the Bragg equations. The average crystallite sizes were determined using the Debye-Scherrer formula assuming a shape factor of 0.9.

The relatively broad peaks of the $HfO_2$ pattern on glass substrate indicate small crystallite size. Analysis of the (111) diffraction peak at ≈31.7° using the Debye–Scherrer formula yields an average crystallite size of 8.27 nm. Based on the pattern of the $HfO_2$ we may safely claim deposition of monoclinic $HfO_2$, space group $P2_1/c$ (ICDD 43–1017 and 65–1142). Spray coated $HfO_2$ films on KBr substrates were further investigated by FTIR. **Figure 6** illustrates the FTIR absorption spectra between 625 cm$^{-1}$ and 825 cm$^{-1}$.

The prominent phonon modes are observed at ≈685 cm$^{-1}$ and ≈770 cm$^{-1}$. The feature at 685 cm$^{-1}$ ($A_u$ symmetry) is attributed to modes of both amorphous and monoclinic $HfO_2$[52] and therefore doesn't provide any further phase identification. The

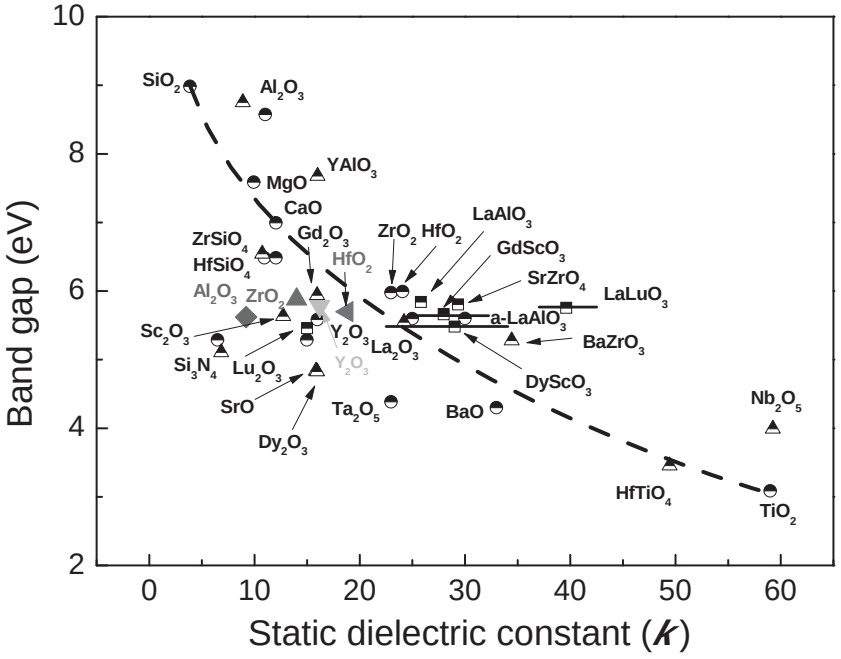


**Figure 4.** Static dielectric constant vs band gap for gate dielectric oxides grown by a wide range deposition methods. Colored (online) data points correspond to spray coated gate dielectrics.

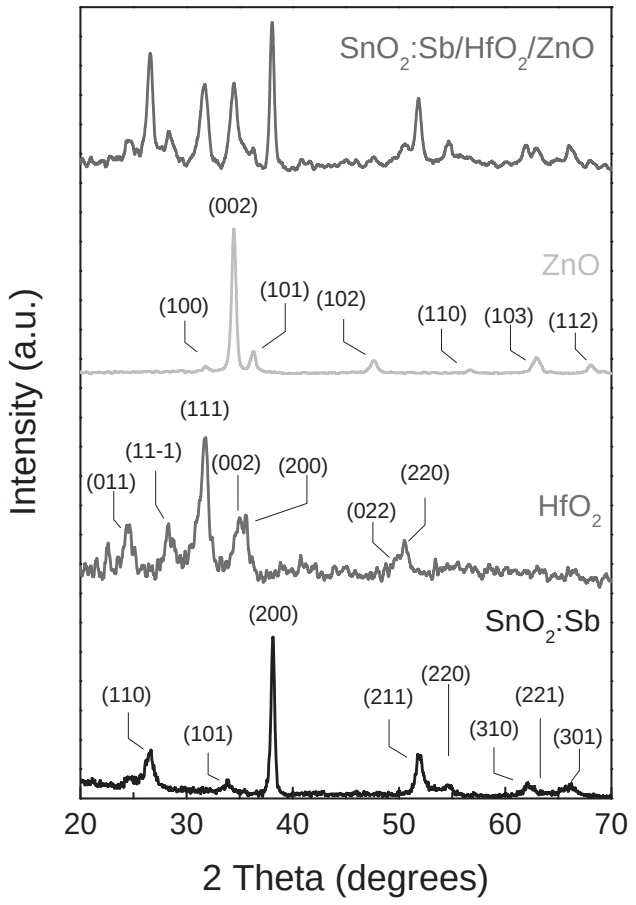


**Figure 5.** GIXRD patterns of $SnO_2$:Sb, $HfO_2$ and ZnO and stack deposited by SP on glass substrates. Indexing of the patterns is based on tetragonal $P4_2/mnm$ $SnO_2$, monoclinic $P2_1/c$ $HfO_2$ and hexagonal $P6_3mc$ ZnO.

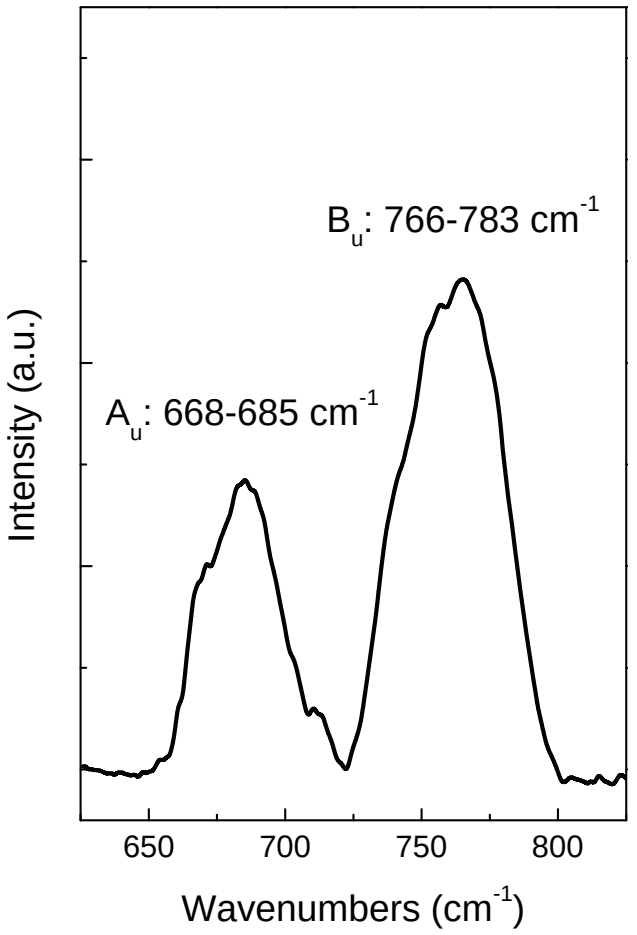


**Figure 6.** FTIR spectra in the region between 625 $cm^{-1}$ and 825 $cm^{-1}$ of $HfO_2$ films deposited by spray pyrolysis on KBr substrates. The feature at ≈770 $cm^{-1}$ further confirms the monoclinic phase of spray coated $HfO_2$.

band at ≈770 $cm^{-1}$ ($A_u$ symmetry) however can be attributed to a characteristic phonon mode of monoclinic $HfO_2$ further confirming the monoclinic phase of our spray coated $HfO_2$ films.[53–55]

Similarly for the spray coated gate electrode, the analysis of the X-ray diffraction patterns revealed that the $SnO_2$:Sb films are one of the pure crystalline tetragonal rutile phase of tin oxide (ICDD41–1445 and 88–0287) of the space group $P4_2/mnm$. No obvious peaks from other antimony oxide phases such as $Sb_2O_5$ or $Sb_2O_3$ were detected. From the XRD patterns it is seen that the $SnO_2$:Sb films show a preferential growth along the (200) orientation. Further indexing of the XRD patters yield an average crystal size of ≈20.98 nm and lattice parameters *a* and *c* of ≈5.245 Å and ≈3.056 Å respectively. As previously reported, spraying of the Zn containing precursor solution at temperatures of ≈400 °C yields polycrystalline ZnO films as also illustrated in Figure 5. The average crystal size of the hexagonal ZnO (space group $P6_3mc$) as determined from the (002) reflection (ICDD 36–1451 and 65–0523), found to be ≈20.3 nm in excellent agreement with previous reports[8,18] and also exhibit a propensity for growth along the (002) direction.

### 2.4. Surface Properties of $SnO_2$:Sb and $SnO_2$:Sb/$HfO_2$/ZnO Stacks

The surface morphologies of $SnO_2$:Sb, $HfO_2$, and ZnO films were investigated by atomic force microscopy (AFM). Topography images of each individual layer are depicted in **Figure 7** and clearly illustrate films of low roughness.

The images presented are the raw images after they have been simply flattened out. Further image processing (e.g., for tip dilation) was omitted as it showed no effect on the image quality. The films' surface roughness was calculated in terms of root-mean-square and found to be ≈5.0 nm for $SnO_2$:Sb considerably higher than those of $HfO_2$ dielectric (≈0.8 nm) and ZnO semiconducting channel (≈1.7 nm). The obvious differences in the grain size (qualitatively consistent with the XRD measurements) indicate for the $HfO_2$ dielectrics that surface morphology is being dominated by the deposition process itself rather than the underlying morphology of the $SnO_2$:Sb layer. Such low surface roughness providing a good interface between the $HfO_2$ and ZnO is promising for the implementation of spray coated films into thin film transistor devices.

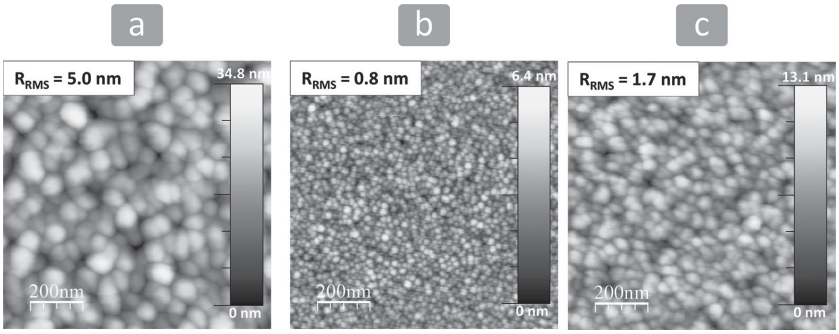


**Figure 7.** AFM and topography images (and RMS roughness inset) of $SnO_2$:Sb deposited on glass, $HfO_2$ on glass/$SnO_2$:Sb and ZnO on glass/$SnO_2$:Sb/$HfO_2$ substrates.

### 2.5. ZnO-based Thin Film Transistors Employing $HfO_2$ Gate Dielectrics

The performance of $HfO_2$ films as gate dielectrics was investigated in a bottom-gate, top-contact (BG–TC) TFT architecture (inset, **Figure 8**a) employing ZnO as then-channel semiconductor. $HfO_2$ was deposited by spray pyrolysis (at ≈400 °C) onto spray pyrolysis-grown $SnO_2$:Sb electrodes followed by the sequential deposition of ZnO, also by spray pyrolysis under ambient conditions. Device fabrication was completed with the deposition of Al source and drain (S/D) electrodes by thermal evaporation under high vacuum ($10^{-7}$ mbar). Figure 8 shows a representative set of transfer and output characteristics obtained from a ZnO TFT ($L$ = 20 µm, $W$ = 2000 µm) based on a ≈100 nm thick $HfO_2$ high-$k$ dielectric. The device exhibits excellent operating characteristics with negligible hysteresis, low voltage operation, high current on/off ratio in excess of $10^7$ and maximum electron mobility of approximately 42 $cm^2 V^{-1} s^{-1}$. This value is considerably increased compared with the ones obtained from spray coated pristine ZnO-based TFTs employing $ZrO_2$, $Y_2O_3$, and $Al_2O_3$ gate dielectrics or spray coated pristine ZnO grown on thermal $SiO_2$.[8,9,17,18]

Given the similarity of the deposition process and device manufacturing we may attribute this electron mobility increase to the improved interface in terms of lattice match between the $HfO_2$ dielectric and ZnO semiconductor, however in this report, we are unable to provide evidence in support of our assumption.

An important yield metric for SP processed TFTs, is the device manufacturing reproducibility. **Figure 9** illustrates the histograms of the mobility and threshold voltage of ZnO-based TFTs employing $HfO_2$ gate dielectrics layers manufactured under the same conditions onto $SnO_2$:Sb and refer to the data obtained from TFTs with $W$ = 2000 µm and $L$ = 20 µm.

Another important aspect is related to the device's transparency. The overall transmittance of the TFT's channel, i.e., glass/$SnO_2$:Sb/$HfO_2$/ZnO stack is depicted in **Figure 10**. The average transmission in the visible range (400–700 nm) was found to be of ≈80%.

## 3. Conclusions

We have demonstrated solution processed $HfO_2$ dielectrics over a large area under ambient conditions at moderate temperatures (≈400 °C) and their implementation in ZnO-based transistors also employing spray coated $SnO_2$:Sb gate electrodes. The physical properties of $HfO_2$ films were investigated using a wide range of characterization techniques that revealed smooth $HfO_2$ films of monoclinic structure, wide band gap, high-$k$, high transparency and low leakage currents. The ZnO-based TFTs that were also manufactured from solutions on top of $HfO_2$ layers showed excellent characteristics, that is, electron mobilities in excess of 40 $cm^2$/Vs, negligible hysteresis, and high on/off current ratios. The devices (after thermal annealing at 100 °C at ambient conditions) showed excellent air and constant bias stress stability (data not shown). In addition, the high reproducibility that was demonstrated indicates the potential for the rapid development of transparent oxide electronics from solutions at low manufacturing cost.

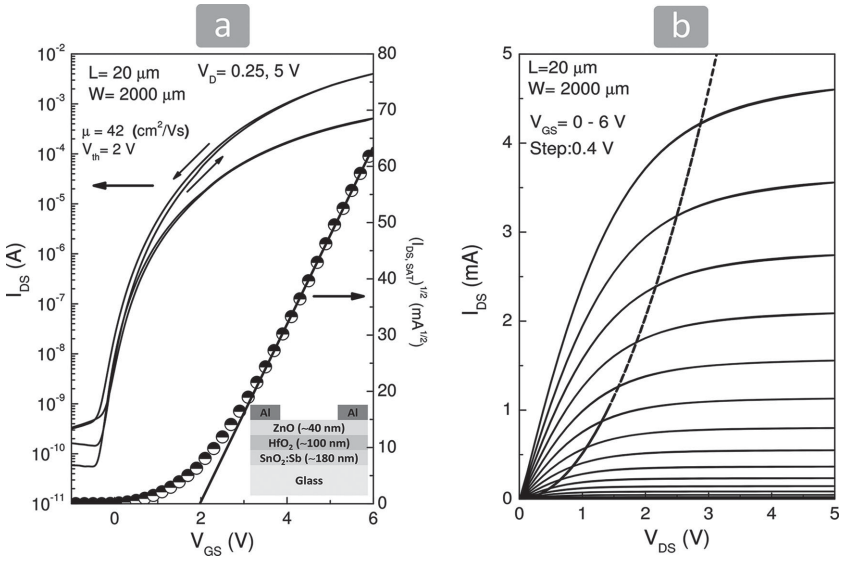


**Figure 8.** a) Linear ($V_{DS}$ = 0.25 V) and saturated ($V_{DS}$ = 5 V) transfer characteristics of bottom-gate, top-contact (inset: architecture employed) TFTs with channel width $W$ = 2000 µm and channel length $L$ = 20 µm, fabricated with spray coated ZnO films on a 151 nF/$cm^2$ $HfO_2$ dielectric by SP. b) Output characteristics of ZnO TFT employing SP deposited $HfO_2$ gate dielectric.

## 4. Experimental Section

*$SnO_2$:Sb, $HfO_2$ and ZnO Deposition by Spray Pyrolysis*: A 20 mg/mL precursor solution of tin chloride ($SnCl_4$) and 5 mg/mL of antimony chloride ($SbCl_3$) was prepared in methanol. Sb doping ([$Sb^{+3}$]/[$Sn^{+4}$+ $Sb^{+3}$]: 2%) was achieved by blending the tin chloride solution with the desired quantity of the antimony chloride solution. Corning

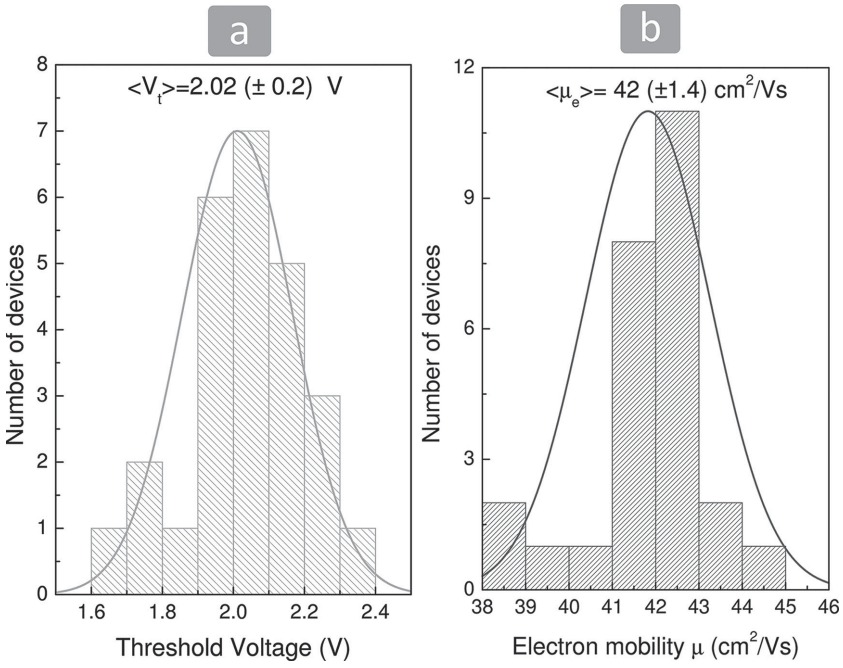


**Figure 9.** Histograms of a) the mobility and b) threshold voltage of ZnO-based TFTs employing $HfO_2$ gate dielectrics that were manufactured under the same conditions onto $SnO_2$:Sb. The data and refer to the data obtained from TFTs with W = 2000 μm and L = 20 μm.

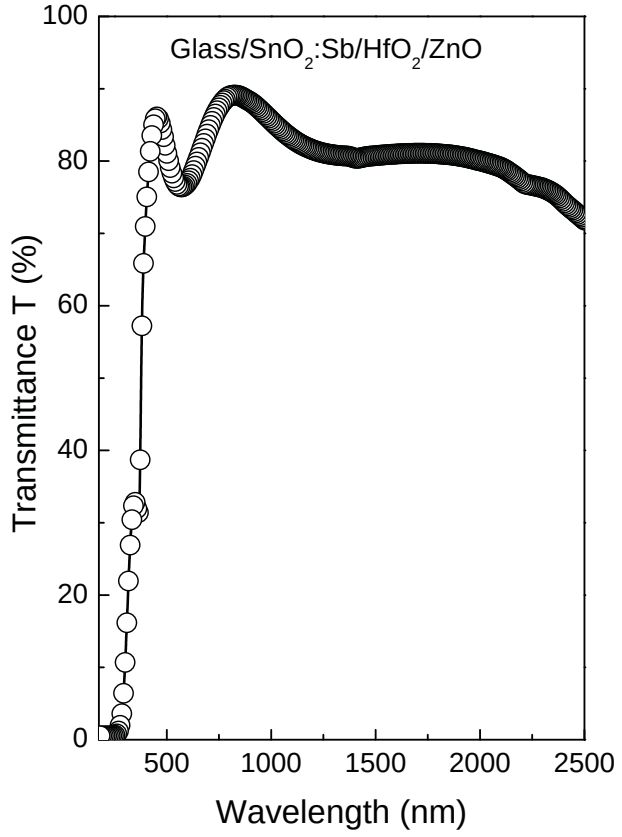


**Figure 10.** The overall transmittance of the TFT's channel i.e., glass/$SnO_2$:Sb/$HfO_2$/ZnO stacks.

1737 glass substrates were kept at 380 °C on a hotplate, while aerosols of the blend were sprayed sporadically onto Corning 1737 glass employing a pneumatic airbrush, held at a vertical distance of about 30 cm. After a period of 10 s, the spraying process was interrupted for 30 s to allow for the vapors to settle onto the sample before the cycle was repeated until films of typical thicknesses of 180 nm were obtained. Similarly, aerosols of a 40 mg/mL hafnium chloride ($HfCl_4$) solution in methanol and ethanol (1:2) were sequentially spray coated at 450 °C onto the $SnO_2$:Sb coated glass. Finally the ZnO semiconducting channels were spray coated on glass/$SnO_2$:Sb/$HfO_2$ (≈100 nm) stacks (kept at 400 °C) from 22 mg/mL zinc acetate ($Zn(CH_3CO_2)_2$) solutions in DI water until films of typical thickness of ≈40 nm were obtained.

*TFTs Fabrication/Characterization*: Bottom Gate–Top Contact (BG–TC) transistors were then fabricated. Aluminum (Al) source and drain (S/D) electrodes (50 nm) were thermally evaporated under high vacuum ($10^{-7}$ mbar) through a shadow mask on the spray coated glass/$SnO_2$:Sb(180 nm)/$HfO_2$(100 nm)/ZnO(40 nm) stacks. Device characterization was performed under high vacuum ($10^{-6}$ mbar), at room temperature. Electrical measurements were carried out using an Agilent B1500A semiconductor parameter analyzer. Electron mobility was extracted from the transfer curves in both the linear and saturation regime using the gradual channel approximation. The devices were thermally annealed at 100 °C in air for 30 min prior the characterization.

*Impedance Spectroscopy*: Impedance spectroscopy measurements on MIM devices (glass/$SnO_2$:Sb/$HfO_2$/Au) were performed using a Wayne Kerr 6550B Precision Impedance Analyzer at frequencies between 20 Hz and 10 MHz applying a 25 mV AC voltage. The Au electrodes were thermally evaporated on $HfO_2$ under high vacuum ($10^{-7}$ mbar) through a shadow mask.

*Atomic Force Microscopy*: Atomic force microscopy images were taken in tapping mode under ambient conditions using a Veeco Dimension 3100 SPM system using a silicon tip of a radius < 10 nm.

*Sheet Resistivity*: The sheet resistivity of glass/$SnO_2$ was measured applying the Four-terminal sensing technique using a Jandel Multi Height Probe system with an Agilent B1500A semiconductor parameter analyzer.

*X-Ray Diffraction*: Grazing Incidence XRD (GIXRD) experiments were performed using a Rigaku Ultima$^+$ diffractometer with $CuK_\alpha$ radiation operating at 40 kV.

*UV–Vis Absorption Spectroscopy*: Optical transmission spectra of $HfO_2$ on quartz and stacks on glass substrates were measured at wavelengths between 175 nm and 2500 nm using an Agilent Cary 5000 spectrometer.

*FTIR*: The FTIR measurements of ZnO films on potassium bromide (KBr) substrates were conducted in transmission mode using a Perkin Elmer system 2000 Fourier transform spectrophotometer at the spectral ranges from 4000–370 $cm^{-1}$ at a spectral resolution of 1 $cm^{-1}$.

*Spectroscopic Ellipsometry*: SE measurements of $HfO_2$ films on intrinsic c-Si were performed in ambient conditions at an incidence angle of 70° using a Jobin–Yvon UVISEL phase modulated system at the spectral range between 1.5 eV and 6 eV.

## Acknowledgements

M.E. is grateful for support from the Ministry of Education Malaysia and Universiti Teknikal Malaysia, Melaka.

Received: August 7, 2014
Revised: September 29, 2014
Published online: November 10, 2014

[1] M. W. J. Prins, K. O. GrosseHolz, G. Muller, J. F. M. Cillessen, J. B. Giesbers, R. P. Weening, R. M. Wolf, *Appl. Phys. Lett.* **1996**, *68*, 3650.
[2] R. L. Hoffman, B. J. Norris, J. F. Wager, *Appl. Phys. Lett.* **2003**, *82*, 733.
[3] K. Nomura, H. Ohta, K. Ueda, T. Kamiya, M. Hirano, H. Hosono, *Science* **2003**, *300*, 1269.
[4] E. Fortunato, P. Barquinha, A. Pimentel, L. Pereira, G. Goncalves, R. Martins, *Phys. Status Solidi* **2007**, *1*, R34.
[5] E. Fortunato, P. Barquinha, R. Martins, *Adv. Mater.* **2012**, *24*, 2945.
[6] P. Barquinha, L. Pereira, G. Goncalves, R. Martins, E. Fortunato, *J. Electrochem. Soc.* **2009**, *156*, H161.
[7] J. Nishii, F. M. Hossain, A. Takagi, T. Aita, K. Saikusa, Y. Ohmaki, I. Ohkubo, S. Kishimoto, A. Ohtomo, T. Fukumura, F. Matsukura, Y. Ohno, H. Koinuma, H. Ohno, M. Kawasaki, *Jpn. J. Appl. Phys.* **2003**, *42*, L347.
[8] G. Adamopoulos, A. Bashir, W. P. Gillin, S. Georgakopoulos, M. Shkunov, M. A. Baklar, N. Stingelin, D. D. C. Bradley, T. D. Anthopoulos, *Adv. Funct. Mater.* **2011**, *21*, 525.
[9] A. Bashir, P. H. Wobkenberg, J. Smith, J. M. Ball, G. Adamopoulos, D. D. C. Bradley, T. D. Anthopoulos, *Adv. Mater.* **2009**, *21*, 2226.
[10] S. R. Thomas, P. Pattanasattayavong, T. D. Anthopoulos, *Chem. Soc. Rev.* **2013**, *42*, 6910.
[11] M. G. Kim, H. S. Kim, Y. G. Ha, J. Q. He, M. G. Kanatzidis, A. Facchetti, T. J. Marks, *J. Am. Chem. Soc.* **2010**, *132*, 10352.
[12] K. K. Banger, Y. Yamashita, K. Mori, R. L. Peterson, T. Leedham, J. Rickard, H. Sirringhaus, *Nat. Mater.* **2010**, *10*, 45.
[13] S. Oertel, M. P. M. Jank, E. Teuber, A. J. Bauer, L. Frey, *Thin Solid Films* **2014**, *28*, 114.
[14] H. Faber, B. Butz, C. Dieker, E. Spiecker, M. Halik, *Adv. Funct. Mater.* **2013**, *23*, 2828.
[15] B. N. Pal, B. M. Dhar, K. C. See, H. E. Katz, *Nat. Mater.* **2009**, *8*, 898.
[16] E. Fortunato, R. Barros, P. Barquinha, V. Figueiredo, S.-H. K. Park, C.-S. Hwang, R. Martins, *Appl. Phys. Lett.* **2010**, *97*, 052105.
[17] G. Adamopoulos, S. Thomas, D. D. C. Bradley, M. A. McLachlan, T. D. Anthopoulos, *Appl. Phys. Lett.* **2011**, *98*, 123503.
[18] G. Adamopoulos, S. Thomas, P. H. Wöbkenberg, D. D. C. Bradley, M. A. McLachlan, T. D. Anthopoulos, *Adv. Mater.* **2011**, *23*, 1894.
[19] H. Liu, J. Sun, Q. Tang, Q. Wan, *Phys. Chem. C* **2010**, *114*, 12316.
[20] C. L. Dezelah, J. Niinisto, K. Kukli, F. Munnik, J. Lu, M. Ritala, M. Leskela, L. Niinisto, *Chem. Vap. Deposition* **2008**, *14*, 358.
[21] R. Engel-Herbert, Y. Hwang, J. Cagnon, S. Stemmer, *Appl. Phys. Lett.* **2009**, *95*, 062908.
[22] S. Stemmer, J.-P. Maria, A. I. Kingon, *Appl. Phys. Lett.* **2001**, *79*, 102.
[23] G. V. Samsonov, *The Oxide Handbook*, IFI/Plenum, New York **1982**.
[24] M. Ritala, K. Kukli, A. Rahtu, P. I. Raisanen, M. Leskela, *Science* **2000**, *288*, 319.
[25] J. Niinistö, M. Mäntymäki, K. Kukli, L. Costelle, E. Puukialinen, M. Ritala, M. Leskelä, *J. Cryst. Growth* **2010**, *312*, 245.
[26] U. Patil, R. Thomas, A. Milanov, R. Bhakta, P. Ehrhart, R. Waser, R. Becker, H. Becker, M. Winter, K. Merz, R. A. Fischer, A. Devi, *Chem. Vap. Deposition* **2006**, 172.
[27] R. Pothiraja, A. Milanov, H. Parala, M. Winter, R. A. Fischer, A. Devi, *Dalton Trans.* **2009**, 654.
[28] L. Pereira, P. Barquinha, E. Fortunato, R. Martins, *Mater. Sci. Eng. B* **2005**, *118*, 210.
[29] F. M. Li, B. C. Bayer, S. Hofmann, J. D. Dutson, S. J. Wakeham, M. J. Thwaites, W. I. Milne, A. J. Flewitt, *Appl. Phys. Lett.* **2011**, *98*, 252903.
[30] F. M. Li, B. C. Bayer, S. Hofmann, S. P. Speakman, C. Ducati, W. I. Milne, A. J. Flewitt, *Phys. Status Solidi B* **2013**, *250*, 957.
[31] S. S. Hullavarad, D. E. Pugel, E. B. Jones, R. D. Vispute, T. Venkatesan, *J. Electron. Mater.* **2007**, *36*, 648.
[32] H. Hu, C. X. Zhu, Y. F. Lu, Y. H. Wu, T. Liew, M. F. Li, B. J. Cho, W. K. Choi, N. Yakovlev, *J. Appl. Phys.* **2003**, *94*, 551.
[33] W. C. Lee, Y. J. Lee, Y. D. Wu, P. Chang, Y. L. Huang, Y. L. Hsu, J. P. Mannaerts, R. L. Lo, F. R. Chen, S. Maikap, L. S. Lee, W. Y. Hsieh, M. J. Tsai, S. Y. Lin, T. Gustffson, M. Hong, J. Kwo, *J. Cryst. Growth* **2005**, *278*, 619.
[34] O. Acton, G. Ting, H. Ma, J. W. Ka, H. L. Yip, N. M. Tucker, A. K. Y. Jen, *Adv. Mater.* **2008**, *20*, 3697.
[35] Z. J. Wang, T. Kumagai, H. Kokawa, M. Ichiki, R. Maeda, *J. Electroceram.* **2008**, *21*, 499.
[36] Y. Aoki, T. Kunitake, A. Nakao, *Chem. Mater.* **2005**, *17*, 450.
[37] J. J. Schneider, R. C. Hoffmann, A. Issanin, S. Dilfer, *Mat. Sci. Eng. B* **2011**, *176*, 965.
[38] J. Tauc, *Optical Properties of Solids* (Ed: F. Abeles), North-Holland, Amsterdam **1971**.
[39] J. Robertson, *J. Vac. Sci. Technol. B* **2000**, *18*, 1785.
[40] W. Mönch, *Surf. Sci.* **1994**, *300*, 928.
[41] J. Robertson, *ECS Transactions* **2009**, *19*, 579.
[42] J. Robertson, *Rep. Prog. Phys.* **2006**, *69*, 327.
[43] W. J. Zhu, Tso-Ping Ma, T. Tamagawa, J. Kim, Y. Di, *IEEE Electr. Device L.* **2002**, *23*, 97.
[44] J. A. Duffy, *Bonding Energy Levels and Bands in Inorganic Solids*, Longman Scientific & Technical, London **1990**.
[45] J. Robertson, *J. Appl. Phys* **2008**, *104*, 124111.
[46] J. Robertson, *Eur. Phys. J. Appl. Phys.* **2004**, *28*, 265.
[47] J. Robertson, *Phys. Status Solidi A* **2010**, *207*, 261.
[48] J. Robertson, *Appl. Surf. Sci.* **2002**, *190*, 2.
[49] D. G. Schlom, J. H. Haeni, *MRS Bull.* **2002**, 198.
[50] J. A. Kittl, K. Opsomer, M. Popovici, N. Menou, B. Kaczer, X. P. Wang, C. Adelmann, M. A. Pawlak, K. Tomida, A. Rothschild, B. Govoreanu, R. Degraev, M. Schaekers, M. Zahid, A. Delabie, J. Meersschaut, W. Polspoel, S. Clima, G. Pourtois, W. Knaepen, C. Detavernier, V. V. Afanas'ev, T. Blomberg, D. Pierreux, J. Swert, P. Fischer, J. W. Maes, D. Manger, W. Vandervorst, T. Conard, A. Franquet, P. Favia, H. Bende, B. Brij, S. Van Elshocht, M. Jurczak, J. Van Houdt, D. J. Wouters, *Microelectronic Eng.* **2009**, *86*, 1789.
[51] E. J. Sonneveld, J. W. Visser, *J. Appl. Cryst.* **1975**, *8*, 1.
[52] L. Koltunski, R. A. B. Devine, *Appl. Phys. Lett.* **2001**, *79*, 320.
[53] M. M. Frank, S. Sayan, S. Dörmann, T. J. Emge, L. S. Wielunski, E. Garfunkel, Y. J. Chabal, *Mater. Sci. Eng. B* **2004**, *109*, 6.
[54] D. A. Neumayer, E. Cartier, *J. Appl. Phys.* **2001**, *90*, 1801.
[55] N. V. Nguyen, A. V. Davydov, D. Chandler-Horowitz, M. M. Frank, *Appl. Phys. Lett.* **2005**, *87*, 192903.